Am J Cancer Res 2025;15(5):2222-2242
www.ajcr.us /ISSN:2156-6976/ajcr0163911

Original Article

Causal impact of genetically determined metabolites on kidney cancer and its subtypes: an integrated mendelian randomization and metabolomic study

Zheng Wang[1*], Zhao Huangfu[1*], Tao Liu[1*], Yuan Li[1,2*], Yuchen Gao[3], Xinxin Gan[1,2], Xiaofeng Wu[1], Shu Chen[4], Xiaomin Li[1], Linhui Wang[1], Xiaofeng Gao[1]

[1]Department of Urology, Changhai Hospital, Naval Medical University, Shanghai 200433, China; [2]School of Health Science and Engineering, University of Shanghai for Science and Technology, Shanghai 200433, China; [3]Department of College of Arts, Sciences, and Engineering, The University of Rochester, Rochester, NY 14627, United States; [4]Key Laboratory of Clothing Design and Technology, Ministry of Education, Donghua University, Shanghai 200051, China. [*]Equal contributors and co-first authors.

Received February 14, 2025; Accepted April 30, 2025; Epub May 15, 2025; Published May 30, 2025

Abstract: Metabolic dysregulation is a hallmark of kidney cancer, yet the causal roles of specific metabolites in its major subtypes remain unclear. This study aimed to elucidate the causal relationships between circulating metabolites and the three primary subtypes of kidney cancer - clear cell renal cell carcinoma (ccRCC), papillary RCC (pRCC), and chromophobe RCC (chRCC) - and to identify potential diagnostic and therapeutic targets. A total of 1,400 circulating metabolites and metabolic ratios were evaluated as exposures, with kidney cancer outcomes derived from the FinnGen database. Genetic instruments were selected from genome-wide association studies (GWAS) and harmonized with outcome data. Mendelian randomization (MR) analyses were conducted using the inverse-variance weighted (IVW) method as the primary approach, supported by multiple sensitivity analyses, including Cochran's Q test, MR-Egger regression, leave-one-out analysis, and MR-PRESSO. To correct for multiple testing, metabolites were stratified into absolute levels and metabolic ratios, and the Benjamini-Hochberg false discovery rate (FDR) procedure was applied separately within each category. Causally associated metabolites were further analyzed via KEGG pathway enrichment. For clinical validation, untargeted metabolomic profiling was performed on paired tumors and adjacent normal tissues from 48 patients with ccRCC. In total, 85 metabolites were found to be causally associated with kidney cancer, including 57 for ccRCC, 71 for pRCC, and 51 for chRCC. After FDR correction, three metabolites remained statistically significant: carnitine (overall RCC: OR = 1.25, P_{FDR} = 0.032), trigonelline (overall RCC: OR = 1.25, P_{FDR} = 0.049), and gamma-glutamylthreonine (chRCC: OR = 2.90, P_{FDR} = 0.012). KEGG analysis revealed significant enrichment in the valine, leucine, and isoleucine biosynthesis pathway for ccRCC ($P = 1.2 \times 10^{-5}$), and pyrimidine metabolism for chRCC ($P = 6.5 \times 10^{-6}$). Metabolomic profiling of ccRCC tissues confirmed aberrant levels of seven metabolites, including elevated 2-hydroxyglutarate (fold change [FC] = 3.1, P = 0.001) and reduced citrate (FC = 0.4, P = 0.001), both associated with disease progression. In conclusion, this integrative study identified carnitine and trigonelline as potential contributors to RCC progression, while gamma-glutamylthreonine appears to be specifically involved in chRCC pathogenesis. Additionally, altered expression of sphingosine 1-phosphate, acetylcarnitine, gamma-glutamylglutamine, and N-acetylcytidine in ccRCC highlights key metabolic disruptions and underscores their potential as novel biomarkers and therapeutic targets in kidney cancer.

Keywords: Metabolomics, kidney cancer, clear cell renal cell carcinoma (ccRCC), Mendelian randomization (MR), metabolic pathways, carnitine, sphingosine

Introduction

Kidney cancer, a malignancy arising primarily from various epithelial cell types within the renal parenchyma, ranks among the most common malignant tumors of the urinary system [1]. Clinically, the majority of kidney cancer cases are asymptomatic in the early stages, with approximately 30% of patients presenting with metastatic disease at diagnosis - a condition associated with poor prognosis [2]. Globally, an estimated 400,000 new cases and 175,000 deaths from kidney cancer occur each year, and both incidence and mortality rates

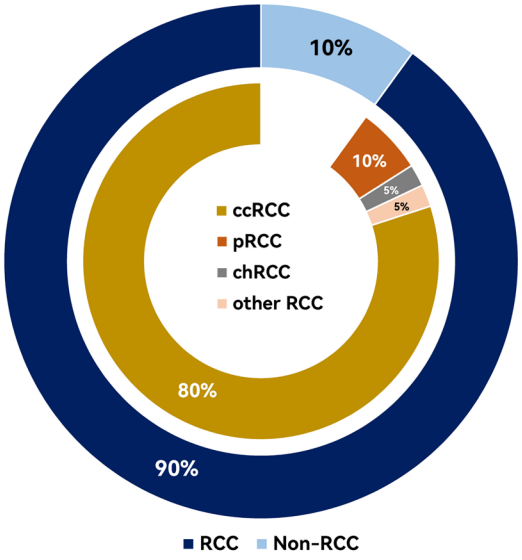

Figure 1. Proportions of pathological subtypes in kidney cancer. The outer ring represents the proportion of kidney cancer cases, with renal cell carcinoma (RCC) accounting for 90% and non-RCC cases comprising 10%. The inner ring further categorizes the RCC cases into subtypes: ccRCC (80%), pRCC (10%), chRCC (5%), and other RCCs subtypes (5%).

have shown a persistent upward trend [3]. This growing burden has spurred increasing research interest in its pathogenesis and clinical management. Although established risk factors-such as smoking, obesity, hypertension, and genetic as well as environmental influences-are known to contribute to the development of kidney cancer, they do not fully explain its rising global incidence [4, 5].

Renal cell carcinoma (RCC) is the most prevalent histological type of kidney cancer, constituting approximately 90% of cases. According to the World Health Organization (WHO) classification, RCC can be broadly categorized into three major subtypes: clear cell RCC (ccRCC), papillary RCC (pRCC), and chromophobe RCC (chRCC) (**Figure 1**) [6]. ccRCC, the dominant subtype, accounts for approximately 70-80% of RCC cases and is characterized histologically by clear cytoplasm attributed to lipid and carbohydrate accumulation. pRCC, the second most prevalent subtype, accounts for approximately 10-15% of RCC cases and exhibits papillary or finger-like tumor projections. In contrast, chRCC, representing approximately 5-7% of RCCs, is distinguished by pale cytoplasm and prominent perinuclear halos. Despite advances in cancer biology, the etiology and molecular underpinnings of RCC remain incompletely understood. This absence of reliable diagnostic biomarkers significantly hampers early detection, subtype differentiation, and the ability to distinguish malignant from benign renal masses, particularly in the preoperative setting.

Metabolomics is a comprehensive study of small-molecule metabolites involved in human biochemical processes. It has emerged as a powerful tool for elucidating disease mechanisms and identifying potential diagnostic or prognostic biomarkers [7, 8]. With recent technological advances, high-throughput metabolomics now enables the detection of hundreds to thousands of metabolites in biological samples such as blood, offering valuable insights into physiological and pathological states [9]. Metabolic dysregulation has been increasingly recognized as a hallmark of kidney cancer, with metabolic reprogramming contributing significantly to tumor initiation and progression [10, 11]. Aberrations in key metabolic pathways-such as glycolysis, fatty acid metabolism, and oxidative stress responses-are frequently observed in urological malignancies, underscoring the relevance of metabolic profiling for uncovering disease-specific vulnerabilities and therapeutic targets [12-15]. However, most existing studies have focused on individual metabolites or specific metabolic classes and have predominantly centered on ccRCC. As a result, comprehensive metabolomics analyses across different kidney cancer subtypes remain scarce. Additionally, these studies are largely observational, establishing associations without addressing the directionality or causality of the observed metabolic alterations.

Mendelian randomization (MR) is an emerging epidemiological method that leverages genetic variants as instrumental variables (IVs) to infer causal relationships between modifiable exposures and clinical outcomes [16]. By capitalizing on the random allocation of alleles during gamete formation - similar to the principle of randomization in controlled trials - MR effectively minimizes confounding and prevents reverse causation, as genetic variants are fixed at conception and remain unaffected by disease processes [17]. Compared with retrospective studies, MR offers more reliable causal inferences and serves as a cost-effective alter-

native to randomized controlled trials, particularly for evaluating long-term exposures and multiple outcomes. This ability to simultaneously analyze various diseases offers valuable insights into disease mechanisms and potential interventions, making MR a crucial tool in epidemiological research [18-20]. Integrating MR with omics-based data, such as metabolomics, further enhances its power to elucidate the molecular basis of disease [21]. This integrated approach provides a detailed understanding of the biochemical processes and pathways influenced by genetic variants, thereby facilitating the formulation of preventive strategies and the identification of potential diagnostic biomarkers. The synergy between genetic and metabolic information not only elucidates the underlying causes of diseases but also paves the way for targeted therapeutic interventions.

In this study, we systematically investigated the genetically determined causal associations between 1,400 metabolites-including metabolite ratios-and the risk of kidney cancer and its major histological subtypes: ccRCC, pRCC, and chRCC. This comprehensive analysis enabled a more refined assessment of the metabolic factors causally linked to each subtype. Beyond enhancing our understanding of the pathogenic mechanisms underlying kidney cancer, our findings reveal distinct metabolic signatures across the three RCC subtypes. These subtype-specific metabolic profiles provide critical insights for the development of precision medicine approaches, including tailored diagnostic biomarkers and targeted therapeutic strategies aligned with the molecular characteristics of each tumor subtype.

Material and methods

Study design

This study employed a multi-step analytical framework integrating genome-wide association study (GWAS), MR, and clinical metabolomics. As illustrated in **Figure 2A**, we first identified suitable GWAS datasets for both exposure variables and outcome variables (**Figure 2A**). Instrumental variables (IVs) were then extracted according to MR assumptions, ensuring minimal risk of reverse causation, elimination of collinearity, and adequate instrument strength (**Figure 2B**). These IVs were harmonized before being applied in MR analyses for each outcome of interest (**Figure 2C**). To ensure the robustness of the results, sensitivity analyses were conducted to evaluate heterogeneity and pleiotropy (**Figure 2D**).

Exposure variables demonstrating statistically significant and robust causal associations were further examined across overall RCC and its three major subtypes to identify both shared and subtype-specific metabolic features (**Figure 2E**). Pathway enrichment analysis was conducted for the subset of causally associated metabolites to elucidate the underlying biological mechanisms (**Figure 2F**). Finally, to validate our findings in a clinical context, we performed untargeted metabolomic profiling using high-resolution mass spectrometry on paired tumor and adjacent normal tissue samples from 48 patients with ccRCC (**Figure 2G**). By integrating these results with positively associated metabolites identified in the ccRCC group, we evaluated their expression patterns in real-world clinical samples.

GWAS summary statistics

Exposure data were derived from the comprehensive genome-wide association study conducted by Chen et al, which analyzed 1,091 blood metabolites and 309 metabolite ratios in a cohort of 8,299 individuals, predominantly of European ancestry [22]. This dataset provides an extensive catalog of genetic variants associated with metabolite levels, offering a valuable resource for metabolomics-based causal inference.

The diagnostic criteria and subtype classification for kidney cancer were based on the WHO criteria for renal tumors [6]. GWAS data for kidney cancer and its subtypes were sourced from the Finngen R10 release. Detailed information on the outcome datasets is listed in **Table 1**. The primary kidney cancer cohort included 2,372 patients diagnosed with malignant neoplasms of the kidney, excluding tumors of the renal pelvis. The case group consisted of 850 females and 1,522 males, with a median age of 66.12 years. The control group comprised 314,193 cancer-free individuals from the FinnGen database. For the RCC subtype analyses, the ccRCC dataset comprised 944 patients (362 females and 582 males) with a median age of 67.48 years. The pRCC group included

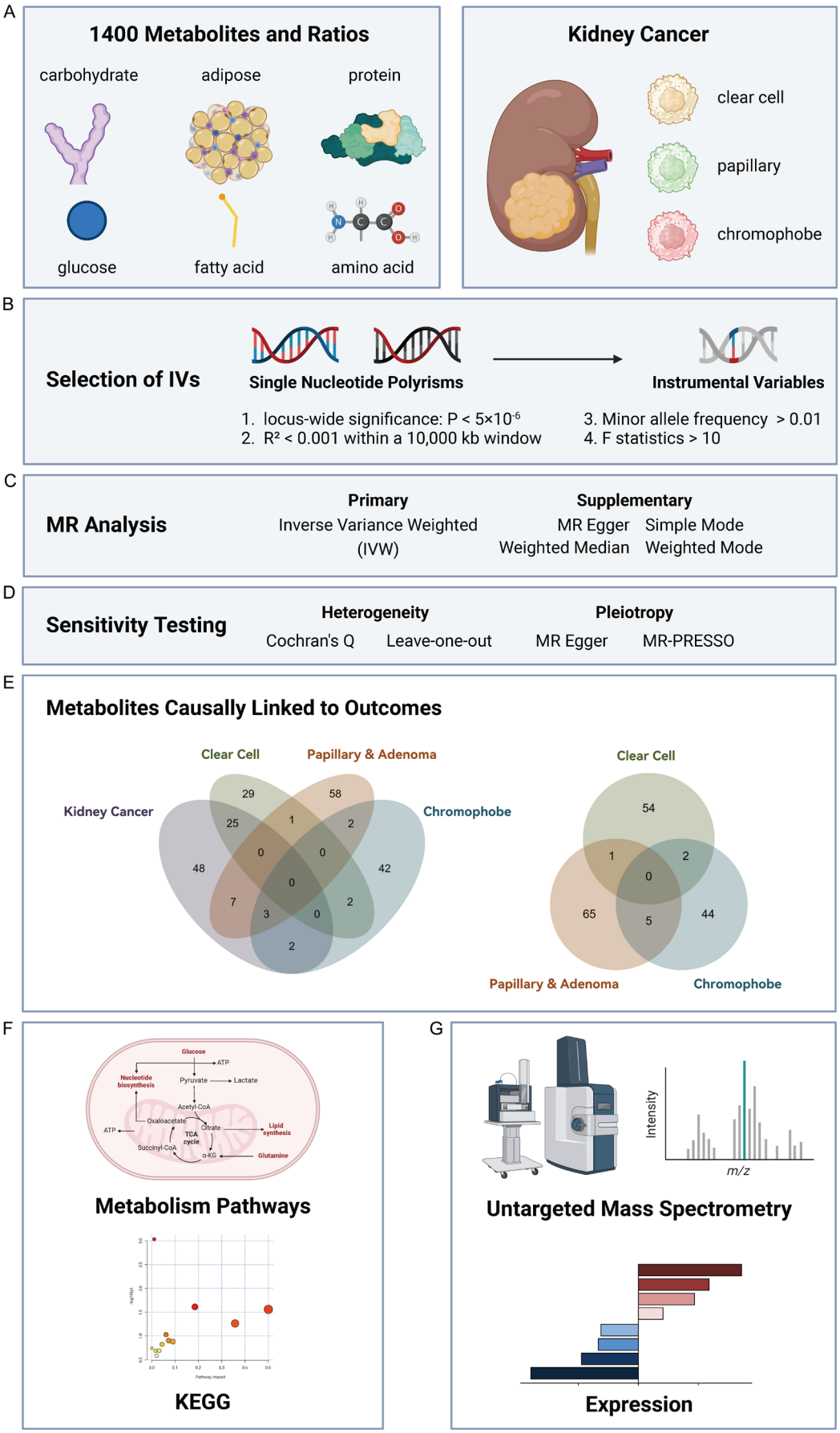
A
1400 Metabolites and Ratios
carbohydrate
adipose
protein
glucose
fatty acid
amino acid
Kidney Cancer
clear cell
papillary
chromophobe
B
Selection of IVs
Single Nucleotide Polyrisms
Instrumental Variables
1. locus-wide significance: P < 5×10-6
2. R² < 0.001 within a 10,000 kb window
3. Minor allele frequency > 0.01
4. F statistics > 10
C
MR Analysis
Primary
Inverse Variance Weighted (IVW)
Supplementary
MR Egger
Simple Mode
Weighted Median
Weighted Mode
D
Sensitivity Testing
Heterogeneity
Cochran's Q
Leave-one-out
Pleiotropy
MR Egger
MR-PRESSO
E
Metabolites Causally Linked to Outcomes
Clear Cell
Papillary & Adenoma
Kidney Cancer
Chromophobe
29
58
25
1
2
0
0
48
42
0
7
3
0
2
2
Clear Cell
54
1
2
0
65
5
44
Papillary & Adenoma
Chromophobe
F
Glucose
ATP
Nucleotide biosynthesis
Pyruvate
Lactate
Acetyl-CoA
Oxaloacetate
Citrate
Lipid synthesis
ATP
TCA cycle
Succinyl-CoA
α-KG
Glutamine
Metabolism Pathways
KEGG
G
Intensity
m/z
Untargeted Mass Spectrometry
Expression

Figure 2. Flow chart of the study design. This figure illustrates the study design for investigating the relationship between metabolites and kidney cancer. A. The exposure of interest includes 1400 metabolites and their ratios, categorized into carbohydrates, adipose tissues, and proteins, along with the kidney cancer subtypes: clear cell (ccRCC), papillary (pRCC), and chromophobe (chRCC). B. Explanation of the criteria for selecting instrumental variables (IVs) via single nucleotide polymorphisms. C. Details of the Mendelian randomization (MR) analysis methods employed, including the primary inverse variance weighting (IVW) method, alongside supplementary methods such as MR Egger, weighted median, simple mode, and weighted mode. D. Lists of the sensitivity testing methods used to assess robustness, including heterogeneity tests (Cochran's Q, leave-one-out) and pleiotropy tests (MR-Egger, MR-PRESSO). E. A Venn diagram illustrating metabolites causally linked to various kidney cancer subtypes, showing both shared and unique metabolites across ccRCC and pRCC. F. Metabolic pathway analysis to understand the functions of the identified metabolites. G. The untargeted mass spectrometry approach was used to analyze the expression differences between tumor tissues and matched normal kidney tissues from 50 kidney cancer patients, aligning the aberrant metabolites with the MR analysis results.

Table 1. Detailed information of outcomes sources

GWAS ID	Traits	Cases	Controls
C3_KIDNEY_NOTRENALPELVIS_EXALLC	Malignant neoplasm of kidney, excluding renal pelvis	2372	314193
C3_KIDNEY_CLEAR_CELL_CARCINOMA_EXALLC	Clear cell adenocarcinoma of the kidney	944	314193
C3_KIDNEY_PAPILLARYADENO_EXALLC	Adenocarcinoma and papillary adenocarcinoma of the kidney	226	314193
C3_KIDNEY_CHROMOPHOBE_EXALLC	Chromophobe cell carcinoma of the kidney	103	314193

226 patients (50 females and 176 males) with a median age of 66.82 years. The chRCC cohort included 103 patients (42 females and 61 males), with a median age of 66.99 years. Control groups for each subtype were selected to match the corresponding case cohorts in terms of demographic characteristics.

Selection of instrumental variables

To ensure the validity and strength of the IVs used in MR analyses, we applied rigorous selection criteria. First, single nucleotide polymorphisms (SNPs) associated with the exposures (metabolites and metabolite ratios) at a significance threshold of $P < 5 \times 10^{-6}$ were identified. Only SNPs with a minor allele frequency (MAF) > 0.01 were included. To minimize bias due to linkage disequilibrium (LD), we applied LD pruning using a threshold of $R^2 < 0.001$ within a 10,000 kb window, based on linkage disequilibrium score regression (LDSC). This step ensured that selected SNPs were independent and not confounded by nearby variants, thereby reducing the risk of horizontal pleiotropy.

When selected SNPs were not available in the outcome GWAS dataset, proxy variants with high LD ($R^2 > 0.8$) were identified and used as substitutes. The strength of each instrument was evaluated using the F-statistic, calculated as: $F = R^2 * (N - 2) / (1 - R^2)$, where R^2 is the proportion of variance in the exposure explained by the SNP and N is the sample size. Only SNPs with F-statistics greater than 10 were retained to avoid weak instrument bias and ensure the reliability of causal inference.

Additionally, the "VariantAnnotation" package was employed to annotate the genetic variants, thereby providing detailed genetic information that facilitated the interpretation of our MR results by linking the variants to established biological functions and pathways. The "phenoscanner" package was used to explore and visualize the relationships between genetic variants and a wide array of phenotypes, thereby enhancing the contextual understanding of our findings and enabling the assessment of pleiotropy and potential confounding factors.

MR analysis

To ensure the robustness and reliability of causal inference, we employed a suite of MR methods. The primary method used was the inverse-variance weighting (IVW) approach, which integrates the individual Wald estimates from each IV using a meta-analysis framework. The technique yields a precision-weighted average of causal estimates [23]. This method also served as the main criterion for determining the presence of causal links. In addition to IVW, several complementary methods were used to validate our findings. MR-Egger regression was employed to identify and adjust for directional (horizontal) pleiotropy, with the intercept term serving as an indicator of such bias [24]. The

weighted median estimator was applied to offer consistent causal estimates even in scenarios where up to 50% of the IVs may be invalid, calculating the median of the distribution of the MR estimates [25]. Furthermore, simple mode and weighted mode methods were used to verify the robustness of the primary findings [26]. These methods provide alternative approaches to estimate causal effects and enhance the robustness of our conclusions.

To correct for multiple testing and control the false discovery rate (FDR), we applied the Benjamini-Hochberg (BH) procedure to IVW-derived *P*-values ($P_{IVW} < 0.05$). Given the large number of metabolite exposures, applying FDR correction across the entire dataset would have been overly conservative and risked overlooking true associations. To address this, exposures were rationally grouped into three biologically and analytically relevant categories: (1) Known metabolite levels, including carbohydrate, lipid, amino acid, organic acid, alkaloid, nucleotide, vitamin, and other classes; (2) Unknown metabolite levels (n = 220); (3) Metabolic ratios (n = 309). FDR correction was then performed independently within each group. This targeted approach enhanced the power to detect meaningful associations while maintaining rigorous control of type I error, enabling the identification of statistically significant metabolites and ratios associated with kidney cancer and its subtypes [27].

Sensitivity analysis

In the MR study, a sensitivity analysis was conducted to identify potential pleiotropy. Cochran's Q test was applied to assess heterogeneity among IVs. A *P*-value greater than 0.05 was interpreted as evidence of low heterogeneity, indicating that variability across the individual SNP estimates was likely due to chance and did not substantially bias the IVW results [28]. To account for the influence of pleiotropy on causal effect estimates, MR-Egger regression was used to detect horizontal pleiotropy [29]. An intercept term close to zero or not statistically significant indicates no directional pleiotropy. Additionally, we applied the MR Pleiotropy RESidual Sum and Outlier (MR-PRESSO) method to identify potential outliers (SNPs with $P < 0.05$) and corrected for horizontal pleiotropy by re-estimating the causal associations after removing these outliers [30]. A leave-one-out analysis was performed by sequentially excluding each SNP. This procedure tested whether the observed causal estimates were driven by any single influential SNP and confirmed the overall stability of the results [31].

Metabolic pathway analysis

To gain insights into the underlying biological mechanisms, we performed metabolic pathway enrichment analysis on metabolites that showed significant causal associations with kidney cancer and its subtypes (PIVW < 0.05) based on the IVW results. The analysis was conducted using the MetaboAnalyst 5.0 platform (https://www.metaboanalyst.ca/) [32]. The pathway analysis module, integrated with the Kyoto Encyclopedia of Genes and Genomes (KEGG) database, was used to identify biologically relevant metabolic pathways potentially implicated in the pathogenesis of overall kidney cancer and the three major subtypes (ccRCC, pRCC, and chRCC).

Patient selection

This prospective study, conducted at Changhai Hospital, included 48 treatment-naive, non-metastatic ccRCC patients undergoing partial or radical nephrectomy. The inclusion criteria were as follows: (1) surgically obtained matched tumor/normal tissue pairs (≥ 200 mg each, with normal tissue sampled ≥ 2 cm from the tumor margin), (2) histopathological confirmation of pure ccRCC (WHO/ISUP grade 1-4) without sarcomatoid/rhabdoid features or mixed histology, (3) M0/N0 status confirmed by preoperative imaging, (4) ECOG performance status of 0-1, and (5) provision of informed consent. Exclusion criteria were: (1) unavailable/inadequate paired tissues (weight < 200 mg), (2) delayed processing (> 30 min post-resection), (3) a history of other malignancies within the past 5 years or active infections, (4) positive surgical margins or prior neoadjuvant therapy, and (5) protocol violations, such as incomplete data or consent withdrawal. All specimens underwent central pathological review and were flash-frozen within 15 minutes of resection. Following quality control, 48 patients (96 paired tissue samples) were ultimately included in the final analysis.

Metabolomic mass spectrometry analysis

Clinical samples were subjected to untargeted metabolomic profiling using high-resolution liquid chromatography-tandem mass spectrometry (LC-MS/MS) equipped with a quadrupole-Orbitrap system (Thermo Fisher Scientific, USA). This approach enabled comprehensive detection and quantification of metabolites in both tumor and adjacent normal tissues. The resulting data were used to characterize global metabolic profiles, assess differences in metabolite expression, and explore patterns indicative of cancer-related metabolic reprogramming. Multivariate analysis techniques were subsequently applied to uncover underlying metabolic signatures differentiating tumor from normal tissues.

Ethics statement

All samples used in this study were obtained from Changhai Hospital, and the study was approved by the hospital's ethics committee (approval number: CHEC2024-234). Written informed consent was obtained from all participants in accordance with the Declaration of Helsinki. The study design adhered to the STROBE-MR guidelines. Ethical approval was granted for each of the original studies contributing data to the database used in this GWAS.

Statistical analysis

All analyses were performed using R (v4.3.1). For MR, the primary method was IVW regression, with random- or fixed-effects models depending on heterogeneity (Cochran's Q test). Sensitivity analyses included MR-Egger, weighted median, simple/weighted mode, and MR-PRESSO (global test $P < 0.05$). Instrument strength was assessed using F-statistics (> 10), and post-hoc power analysis confirmed > 80% power to detect OR ≥ 1.25 at $\alpha = 0.05$. FDR correction was applied within metabolite categories. KEGG pathway enrichment was performed using MetaboAnalyst 5.0 ($P < 0.05$ threshold). Results are presented with exact *P*-values, 95% confidence intervals (CIs), and effect sizes.

For metabolomics, LC-MS/MS data were normalized using probabilistic quotient normalization and log2-transformed. Tumor versus matched adjacent tissues (n = 48) were compared using paired t-tests (mean ± SD) for normally distributed data (Shapiro-Wilk $P > 0.05$), or Wilcoxon signed-rank tests (median and IQR) otherwise. Variance homogeneity was assessed by Levene's test. Multi-group comparisons were analyzed using one-way ANOVA with Tukey's HSD test post-hoc for pairwise comparisons. Statistical significance was set at $P < 0.05$ for all tests (two-tailed). Results are presented with exact *P*-values, 95% confidence intervals (CIs), and effect sizes. PCA and PLS-DA were used to assess global metabolic profiles, with VIP > 1.0 indicating significance. Differential expression was defined as log2 fold change > |1| and $P < 0.05$.

Results

Selection of instrumental variables and MR analysis

We conducted an MR analysis to assess the causal effects of circulating metabolites on the overall incidence of kidney cancer and its three major subtypes (ccRCC, pRCC, and chRCC). All IVs demonstrated F-statistics greater than 10, ensuring robustness and mitigating weak instrument bias. Detailed information on the IVs used for exposure is listed in Table S1. The causal effects of the genetic variants on the outcomes are illustrated in Figure S1.

Our analysis identified a total of 264 metabolites significantly associated with kidney cancer and its subtypes (PIVW < 0.05), with 85 linked to kidney cancer (**Figure 3**), 57 to ccRCC (**Figure 4**), 71 to pRCC (**Figure 5**), and 51 to chRCC (**Figure 6**). The detailed *p*-values and odds ratios (ORs) of these metabolites are listed in Table S2. Several metabolites were found to act as protective factors. For kidney cancer, 3-hydroxymyristate was associated with a reduced risk (OR = 0.777, 95% CI: 0.624-0.966, P = 0.023). For ccRCC, 4-methylguaiacol sulfate provided protective effects (OR = 0.740, 95% CI: 0.550-0.995, P = 0.046). For pRCC, the mannose-to-mannitol-to-sorbitol ratio significantly reduced risk (OR = 0.399, 95% CI: 0.202-0.786, P = 0.007), and 1-linoleoylglycerol (18:2) levels showed notable protection (OR = 0.212, 95% CI: 0.080-0.558, P = 0.001). In contrast, several metabolites were identified as risk factors. For kidney cancer, increased levels of 3-methyladipate were associated with elevated risk (OR = 1.322, 95% CI: 1.076-1.624, P

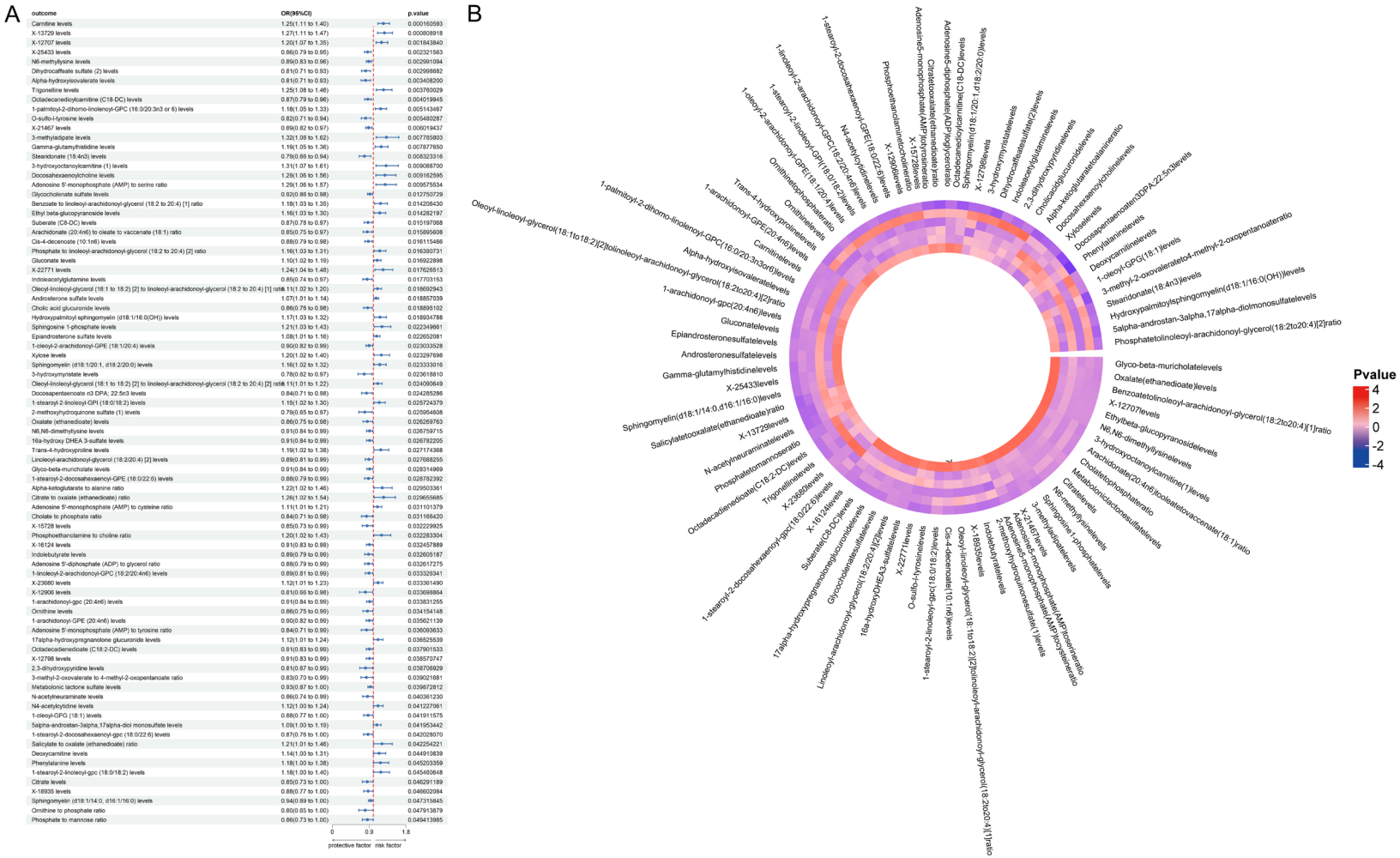

Figure 3. MR results of positive metabolites in kidney cancer. This figure shows the metabolites associated with kidney cancer. A. A forest plot displaying the names of the metabolites, their odds ratios (ORs) with 95% confidence intervals (CIs), and *P* values. The plot shows the strength and statistical significance of each metabolite in relation to kidney cancer. B. A circular heatmap showing the *P*-values of these metabolites, with colors indicating significance levels (red for higher significance and blue for lower significance).

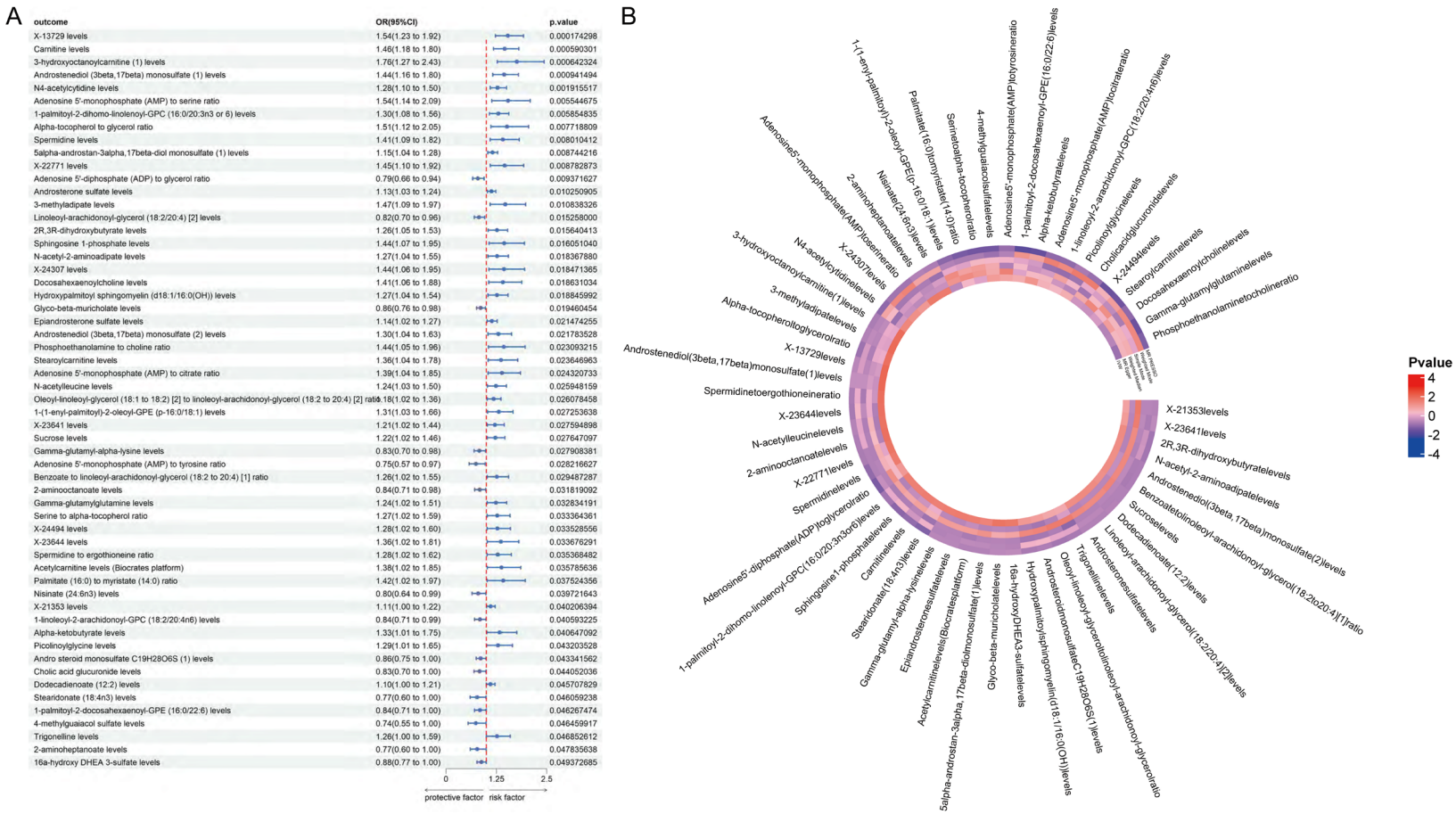

Figure 4. MR results of positive metabolites in Clear Cell Renal Cell Carcinoma (ccRCC). This figure shows the metabolites associated with kidney cancer. A. A forest plot displaying the names of the metabolites, their odds ratios (ORs) with 95% confidence intervals (CIs), and *P* values. The plot shows the strength and significance of each metabolite's association with ccRCC. B. A circular heatmap showing the *P*-values of these metabolites, with colors indicating significance levels (red for higher significance and blue for lower significance).

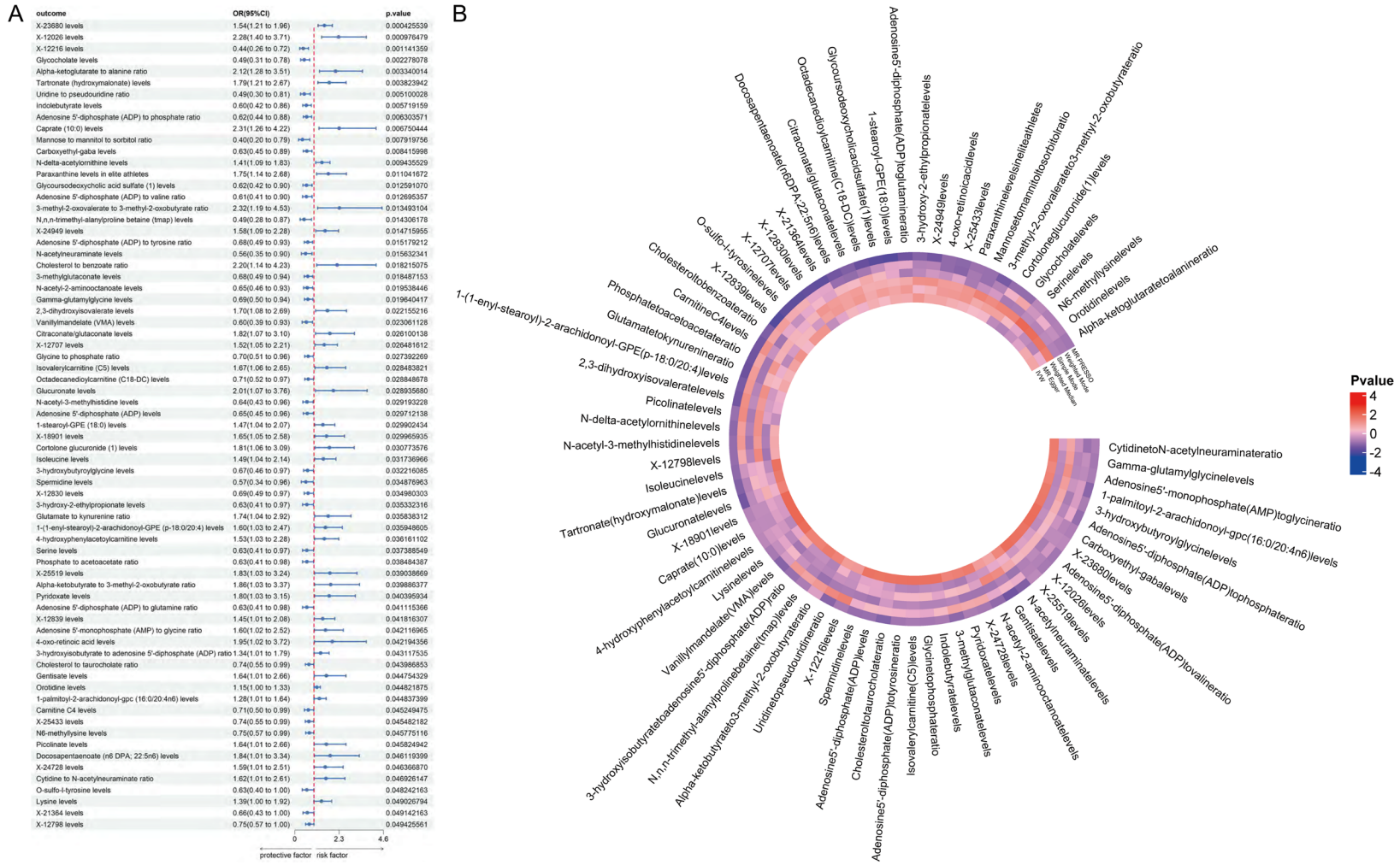

Figure 5. MR results of positive metabolites in Papillary Renal Cell Carcinoma (pRCC). This figure shows the metabolites associated with kidney cancer. A. A forest plot displaying the names of the metabolites, their odds ratios (ORs) with 95% confidence intervals (CIs), and *P* values. The plot shows the strength and significance of each metabolite's association with pRCC. B. A circular heatmap showing the *P*-values of these metabolites, with colors indicating significance levels (red for higher significance and blue for lower significance).

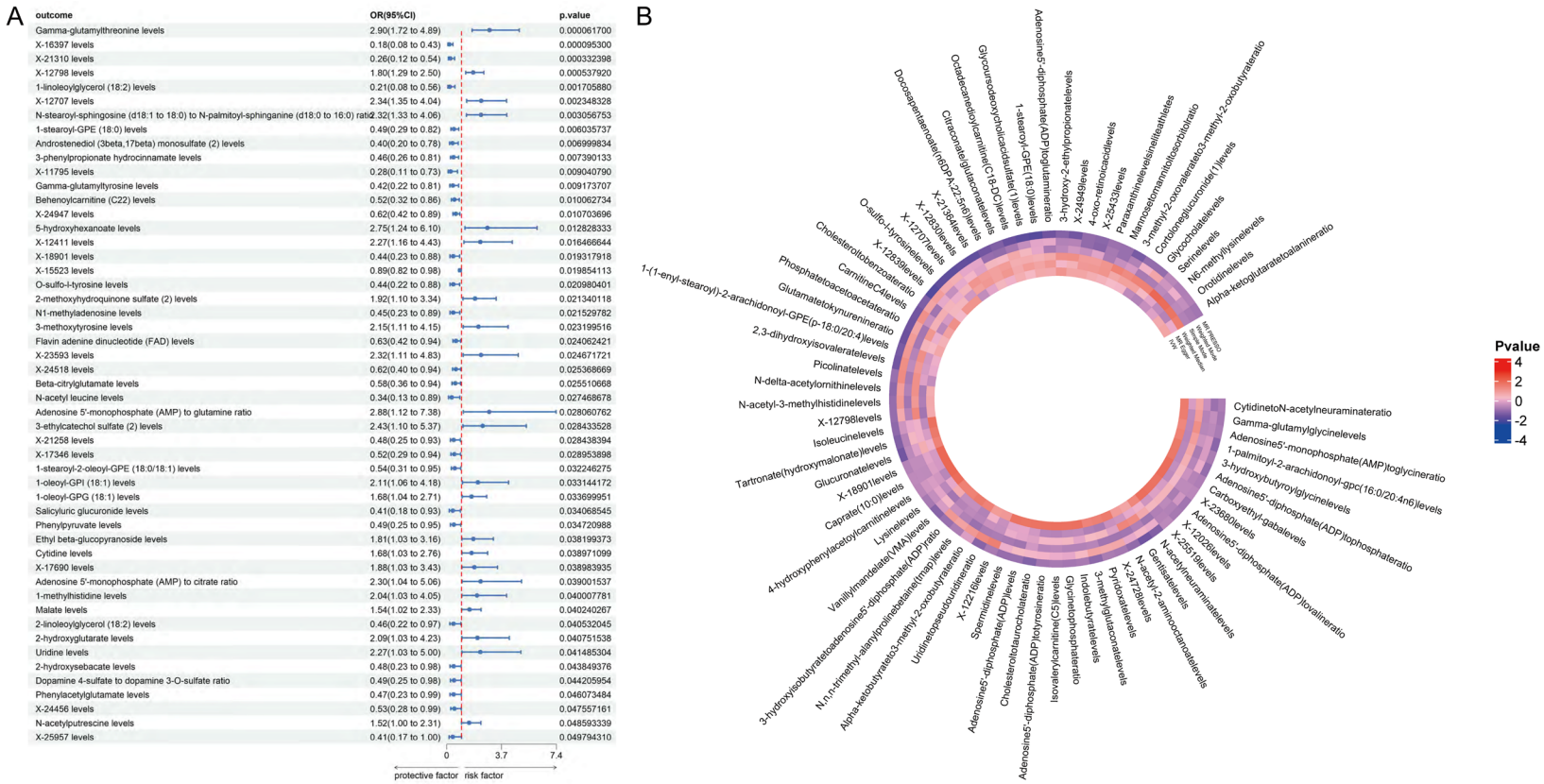

Figure 6. MR results of positive metabolites in Chromophobe Renal Cell Carcinoma (chRCC). This figure shows the metabolites associated with kidney cancer. A. A forest plot displaying the names of the metabolites, their odds ratios (ORs) with 95% confidence intervals (CIs), and *P* values. The plot shows the strength and significance of each metabolite's association with chRCC. B. A circular heatmap showing the *P*-values of these metabolites, with colors indicating significance levels (red for higher significance and blue for lower significance).

Table 2. Significant metabolites identified by multiple two-sample mendelian randomization after FDR correction

Outcome	Exposure	SNPs	Method	Beta	Se	P_{raw}	P_{FDR}	OR (95% CI)	$P_{Heterogeneity}$	$P_{Pleiotropy}$
Kidney Cancer	Carnitine	25	IVW	0.222	0.059	1.606E-04	0.032	1.249 (1.113-1.402)	0.536	
			MR-Egger	0.245	0.098	0.020		1.278 (1.054-1.550)	0.590	
			Weighted median	0.223	0.085	0.009		1.250 (1.057-1.477)		
			Simple mode	0.054	0.160	0.741		1.055 (0.770-1.445)		
			Weighted mode	0.205	0.083	0.022		1.227 (1.042-1.446)		
			MR-PRESSO							0.719
Kidney Cancer	Trigonelline	25	IVW	0.226	0.078	0.004	0.049	1.253 (1.076-1.459)	0.133	
			MR-Egger	0.276	0.127	0.041		1.318 (1.027-1.691)	0.113	
			Weighted median	0.262	0.104	0.012		1.300 (1.059-1.595)		
			Simple mode	0.198	0.177	0.275		1.219 (0.861-1.727)		
			Weighted mode	0.211	0.132	0.122		1.235 (0.954-1.599)		
			MR-PRESSO							0.574
chRCC	Gamma-glutamylthreonine	37	IVW	1.066	0.266	6.170E-05	0.012	2.903 (1.723-4.889)	0.352	
			MR-Egger	1.225	0.460	0.012		3.406 (1.383-8.390)	0.303	
			Weighted median	1.220	0.478	0.011		3.388 (1.327-8.653)		
			Simple mode	1.940	0.735	0.012		6.957 (1.649-29.359)		
			Weighted mode	1.214	0.447	0.010		3.366 (1.402-8.080)		
			MR-PRESSO							0.523

MR: Mendelian randomization; SNPs: single nucleotide polymorphisms; Se: standard error; OR: odds ratio; CI: confidence ratio; chRCC: chromophobe renal cell carcinoma; IVW: Inverse Variance Weighted; MR-Egger: Mendelian Randomization-Egger; MR-PRESSO: Mendelian Randomization Pleiotropy RESidual Sum and Outlier.

= 0.007). For ccRCC, 3-hydroxyoctanoylcarnitine posed a significant risk (OR = 1.758, 95% CI: 1.271-2.431, P < 0.001). For pRCC, the 3-methyl-2-oxovalerate-to-3-methyl-2-oxobutyrate ratio was associated with an increased risk (OR = 2.322, 95% CI: 1.190-4.531, P = 0.013), and gamma-glutamylthreonine significantly increased the risk (OR = 2.902, 95% CI: 1.723-4.889, P < 0.001). The complete MR analysis results, including all exposures and outcomes, along with calculations from the IVW method and various corroborative methods, are detailed in Table S3 and Figure S2.

With respect to the overlap of metabolites associated with different outcomes, our analysis identified 29 metabolites specific to ccRCC, 58 unique to pRCC, and 42 metabolites exclusively associated with chRCC (**Figure 2E**). Further detailed analysis revealed distinct associations between the subtypes (Table S4). Notably, spermidine levels were elevated in both ccRCC and pRCC but not in kidney cancer or chRCC. Levels of androstenediol (3β, 17β) monosulfate and the adenosine 5'-monophosphate (AMP)-to-citrate ratio were higher in ccRCC and chRCC compared to kidney cancer or pRCC. Additionally, levels of 1-stearoyl-GPE (18:0) and X-18901 were increased in pRCC and chRCC but not in kidney cancer or ccRCC.

To address multiple comparisons across 1,400 metabolite exposures, we applied FDR correction separately for each metabolite category (Table S5). After adjustment, three metabolites remained statistically significant (**Table 2**). For overall kidney cancer, both carnitine levels (β = 0.222, $P_{RAW} = 1.61 \times 10^{-4}$; $P_{FDR} = 0.032$) and trigonelline levels (β = 0.226, $P_{RAW} = 0.0038$; $P_{FDR} = 0.049$) showed significant associations with increased risk. In chRCC, gamma-glutamylthreonine levels exhibited a robust causal effect (β = 1.066, $P_{RAW} = 6.17 \times 10^{-5}$; $P_{FDR} = 0.012$). These findings highlight the potential roles of carnitine, trigonelline, and gamma-glutamylthreonine in renal carcinogenesis after rigorous multiple testing adjustments. Other metabolites that did not survive FDR correction may represent potential candidates requiring further validation in larger cohorts.

Sensitivity analysis

The sensitivity analysis was conducted using Cochran's Q test and MR-Egger regression to evaluate heterogeneity (Table S6) and pleiotropy (Table S7 and Figure S3) among the metabolites identified as positively associated with kidney cancer and its subtypes in the previous MR analysis. The metabolites exhibiting both heterogeneity and pleiotropy are listed in **Table 3**.

Table 3. Positive metabolites (P_{IVW} < 0.05) exhibiting heterogeneity and pleiotropy

Outcome	Exposure	Heterogeneity				Pleiotropy	
		Q Statistics		P		Egger Intercept	P
		MR-Egger	IVW	MR-Egger	IVW		
Kidney Cancer	Glycocholate levels	50.74	50.78	0.032	0.041	-0.011	0.872
pRCC	1-oleoyl-GPG (18:1) levels	36.8	38.19	0.034	0.033	-0.022	0.361
Kidney Cancer	Mannose to mannitol to sorbitol ratio	22.65	27.95	0.253	0.111	0.217	0.048
Kidney Cancer	Cytidine to N-acetylneuraminate ratio	20.20	24.70	0.782	0.591	-0.153	0.043
ccRCC	X-23641 levels	29.35	34.26	0.344	0.192	-0.056	0.043
ccRCC	Benzoate to linoleoyl-arachidonoyl-glycerol (18:2 to 20:4) ratio	6.86	11.47	0.940	0.718	-0.081	0.050*
pRCC	N4-acetylcytidine levels	29.85	38.03	0.625	0.291	0.04	0.007
pRCC	3-methyladipate levels	13.17	17.95	0.265	0.790	-0.055	0.046
pRCC	Docosahexaenoylcholine levels	19.68	27.55	0.093	0.529	0.06	0.015

MR-Egger: Mendelian Randomization-Egger; IVW: Inverse Variance Weighted; pRCC: Papillary Renal Cell Carcinoma; ccRCC: Clear Cell Renal Cell Carcinoma; GPG: Glycerophosphoglycerol. *Note: The original *P*-value was 0.0496679934170218. After rounding, even when retaining up to eight decimal places, the *P*-value is rounded to 0.050. This indicates that in the actual report, the *P*-value will not be less than 0.05, even with more decimal places.

For the 85 metabolites associated with kidney cancer, Cochran's Q test indicated significant heterogeneity in the levels of 1-oleoyl-glycerophosphoglycerol (GPG) (18:1) (P = 0.033). MR-Egger regression revealed pleiotropy in the levels of N4-acetylcytidine (P = 0.007), docosahexaenoylcholine (P = 0.015), and 3-methyladipate (P = 0.046). Among the 57 metabolites linked to ccRCC, no significant heterogeneity was observed (P > 0.05), while pleiotropy was detected in the benzoate-to-linoleoyl-arachidonoyl-glycerol ratio (P < 0.05), with the remaining metabolites exhibiting no pleiotropy (P > 0.05). In pRCC, Cochran's Q test indicated heterogeneity in glycocholate levels (P = 0.041), and MR-Egger regression revealed pleiotropy in the cytidine-to-N-acetylneuraminate ratio and the mannose-to-mannitol to sorbitol ratio (P = 0.043 and P = 0.048, respectively). For the 51 metabolites associated with chRCC, no heterogeneity or pleiotropy was detected (P > 0.05).

MR-PRESSO analysis was performed to assess potential horizontal pleiotropy and identify outliers among the metabolites associated with the outcomes. For most outcomes, no positive metabolites exhibited horizontal pleiotropy (Table S8). However, in kidney cancer, exposure to glycocholate exhibited a global test *P*-value of 0.045, indicating the presence of outliers that may have impacted the reliability of the results. Additionally, a leave-one-out analysis was performed on all exposures to assess the robustness of the findings, confirming the stability of the results (Figure S4).

Metabolic pathway analysis

Metabolic pathway analysis of the tested metabolites revealed several pathways significantly associated with kidney cancer subtypes. Metabolites linked to kidney cancer were predominantly enriched in pathways such as lysine degradation (P < 0.001), arginine and proline metabolism (P = 0.024), and the biosynthesis of phenylalanine, tyrosine, and tryptophan (P = 0.027), as illustrated in **Figure 7A**. Specifically, valine, leucine, and isoleucine biosynthesis were significantly associated with the incidence of ccRCC (P = 0.025) (**Figure 7B**). In pRCC, metabolic pathways involving valine, leucine, and isoleucine biosynthesis exhibited marginal significance (P = 0.054) (**Figure 7C**). Furthermore, pathways related to pyrimidine metabolism (P = 0.019), phenylalanine, tyrosine, and tryptophan biosynthesis (P = 0.022), riboflavin metabolism (P = 0.022), and phenylalanine metabolism (P = 0.044) were associated with the occurrence of chRCC (**Figure 7D**).

Untargeted metabolomic mass spectrometry analysis

To validate the clinical relevance of our analytical results, untargeted metabolomic profiling was performed using mass spectrometry on paired cancerous and adjacent non-cancerous tissues from 48 patients with early-stage, non-metastatic ccRCC. The cohort consisted of 30 males and 18 females, with a mean age of 57 years, an average BMI of 24.07, and a mean maximum tumor diameter of 4.27 cm (**Table 4**). Differential expression analysis of metabolites

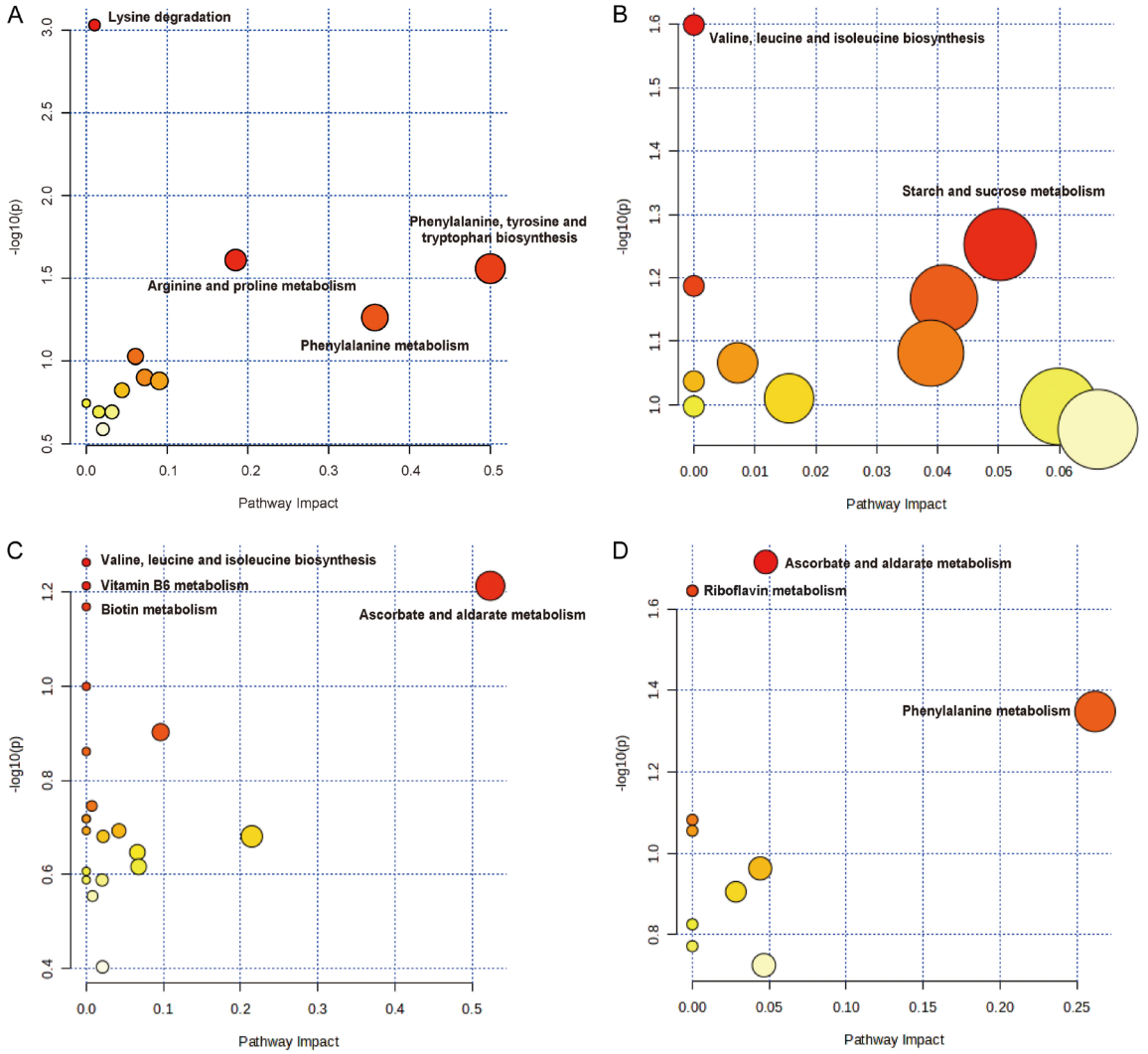

Figure 7. Metabolic pathway analysis for kidney cancer and its subtypes. This figure illustrates the pathway impact analysis across different types of kidney cancer, highlighting the key metabolic pathways associated with each subtype. A. Overall pathway impact for kidney cancer, showing significant pathways such as lysine degradation; arginine and proline metabolism; phenylalanine, tyrosine, and tryptophan biosynthesis, as well as phenylalanine metabolism. B. Metabolic pathways affected in clear cell renal cell carcinoma (ccRCC), with notable pathways including valine, leucine, and isoleucine biosynthesis, and starch and sucrose metabolism. C. Pathway impact specific to papillary renal cell carcinoma (pRCC), highlighting key pathways such as valine, leucine, and isoleucine biosynthesis, vitamin B6 metabolism, biotin metabolism, and ascorbate and aldarate metabolism. D. Pathway impact for chromophobe renal cell carcinoma (chRCC), identifying important pathways including ascorbate and aldarate metabolism, phenylalanine, tyrosine, and tryptophan biosynthesis, riboflavin metabolism, and phenylalanine metabolism. The x-axis represents the pathway impact score, indicating the overall impact of each metabolic pathway on the disease, whereas the y-axis represents the significance level of each pathway, with higher values indicating more significant pathways. The size of the circles indicates the magnitude of the pathway impact, with larger circles representing the pathways with greater impact. The colors of the circles represent the level of significance, with red indicating the most significant pathways and yellow indicating the least significant.

between tumor and paracancerous tissues was conducted to further validate the GWAS findings derived from the MR analysis (**Figure 8**). Notably, we integrated the metabolomic expression profiles with the MR-identified metabolites exhibiting causal relationships-both risk-associated (positively correlated) and protective (negatively correlated)-thereby establishing convergent evidence from both genetic causality and tissue-level dysregulation.

Eight metabolites were found to overlap between our metabolomic profiling and MR analysis, with four exhibiting high expression

Table 4. Clinical characteristics of ccRCC patients in metabolomics analysis

Parameters	Patients (n = 48)
Age (median, IQR)	57.0 ± 15.5
BMI (kg/m^2), (mean, SD)	24.07 ± 2.90
Gender, n (%)	
Male	30 (65.5)
Female	18 (37.5)
Tumor laterality, n (%)	
Left	25 (52.1)
Right	23 (47.9)
Maximum tumor diameter (cm), (mean, SD)	4.27 ± 1.53
T stage, n (%)	
T_{1a}	25 (52.0)
T_{1b}	21 (43.8)
T_2	2 (4.2)
WHO/ISUP grade, n (%)	
I	2 (2.1)
II	43 (89.6)
III	4 (8.3)

IQR: Interquartile range; SD: Standard deviation; WHO/ISUP: World Health Organization/International Society of Urological Pathology Grading System; BMI: Body mass index.

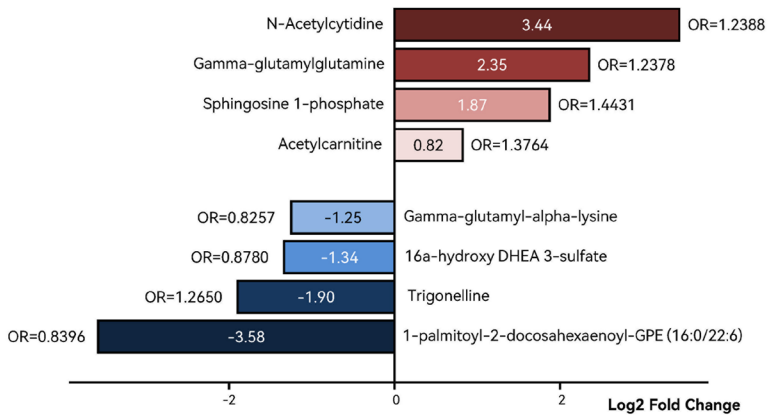

Figure 8. Metabolites with causal relationships and differential expression in Clear Cell Renal Cell Carcinoma (ccRCC) patients. This figure illustrates metabolites that exhibit a causal relationship with ccRCC, as identified by Mendelian randomization (MR) analysis, and show significant differential expression between cancerous and adjacent noncancerous tissues as determined by untargeted mass spectrometry. The bar plot presents the log2-fold change (log2 FC) of each metabolite, with positive values indicating higher expression in cancerous tissues and negative values indicating higher expression in non-cancerous tissues. The odds ratios (ORs) with 95% confidence intervals, derived from the MR analysis, are displayed alongside the bars, showing the strength of the association between each metabolite and ccRCC.

and four showing low expression in tumor tissues. The four highly expressed metabolites, identified as risk factors in the MR analysis, included N-acetylcytidine (log2 FC = 3.441), gamma-glutamylglutamine (log2 FC = 2.352), sphingosine 1-phosphate (log2 FC = 1.873), and acetylcarnitine (log2 FC = 0.823). Among the four metabolites significantly downregulated in tumor tissues, three were identified as protective factors according to MR analysis: 1-palmitoyl-2-docosahexaenoyl-GPE (16:0/22:6) (log2 FC = -3.584), 16a-hydroxy DHEA 3-sulfate (log2 FC = -1.337), and gamma-glutamyl-alpha-lysine (log2 FC = -1.249). Trigonelline, identified as a risk factor despite its lower expression (log2 FC = -1.898), further supported the findings.

Discussion

Study overview and novelty

This study presents an integrated analysis that identifies 85 metabolites associated with kidney cancer, with 57 linked to ccRCC, 71 to pRCC, and 51 to chRCC. After FDR correction, carnitine and trigonelline remained significant for overall kidney cancer, while gamma-glutamylthreonine exhibited the strongest association with chRCC. Metabolic pathway analysis revealed significant enrichment of kidney cancer-associated metabolites in several key metabolic pathways, with distinct associations observed for the subtypes of kidney cancer. In validation experiments using ccRCC patient samples, we identified four upregulated metabolites that promoted tumor growth and three downregulated metabolites that were negatively associated with cancer development. This is the first study to comprehensively integrate MR analysis with metabolomics to investigate the causal relationships between

circulating metabolites and kidney cancer, while distinguishing the distinct metabolic characteristics of its subtypes-ccRCC, pRCC, and chRCC. Additionally, these findings were validated in real-world patient tissue samples, providing direct evidence of these metabolites' relevance in vivo. By comparing the metabolic profiles of different pathological subtypes, we were able to identify the metabolic characteristics associated with the disease. Importantly, the validation with patient tissue samples underscores the potential of these metabolites as both biomarkers and therapeutic targets, particularly for ccRCC, the most prevalent type of kidney cancer.

Subtype-specific causal metabolites and mechanisms

In our study, three metabolites-gamma-glutamylthreonine, carnitine, and trigonelline-were found to exhibit significant associations with RCC risk after rigorous multiple testing correction. These findings shed light on distinct metabolic pathways that may drive renal carcinogenesis, particularly in chRCC. Carnitine, a key mediator of fatty acid oxidation (FAO), was associated with increased overall RCC risk, supporting the FAO-dependency model in hypoxic RCC [33]. Carnitine palmitoyltransferase 1A (CPT1A), the rate-limiting enzyme in FAO, is upregulated in clear cell RCC and correlates with advanced disease [34]. Our results suggest that elevated carnitine levels may facilitate lipid catabolism to fuel tumor growth, which is consistent with preclinical studies showing that CPT1A inhibition suppresses RCC proliferation [35]. Trigonelline, a coffee-derived alkaloid, was nominally associated with RCC risk, which contrasts with its reported antitumor effects in vitro [36]. This discrepancy may arise from its context-dependent actions. While trigonelline exhibits antioxidant properties at low doses, its metabolite N-methylnicotinamide (NMN) can deplete cellular NAD^+ pools, impair DNA repair, and promote genomic instability [37]. Additionally, trigonelline may activate the aryl hydrocarbon receptor (AhR) pathway, which is aberrantly upregulated in RCC and drives IL-6-mediated tumor progression [38]. Population-based studies have similarly linked high trigonelline exposure to increased cancer risk, highlighting the need to explore dose-response relationships and host factors such as smoking and gut microbiota composition [39]. Gamma-glutamylthreonine, a glutathione (GSH)-related metabolite, showed the strongest association with chRCC. This aligns with the unique metabolic profile of chRCC, which is characterized by mitochondrial enrichment and heightened oxidative stress [40]. Gamma-glutamyl peptides play a crucial role in extracellular GSH recycling, a process essential for maintaining redox homeostasis in tumors [41]. In chRCC, overexpression of glutathione peroxidase 4 (GPX4) has been linked to resistance to ferroptosis, a form of cell death triggered by lipid peroxidation [42]. Elevated levels of gamma-glutamylthreonine may thus reflect an adaptive GSH metabolism that supports mitochondrial activity and tumor survival [43]. Targeting this pathway with GSH synthesis inhibitors, such as buthionine sulfoximine, could potentially exploit this vulnerability in chRCC [44].

The metabolic landscape of renal cell carcinoma subtypes reveals both shared and distinct mechanisms driven by genetic and microenvironmental factors. Carnitine and its derivatives, such as acetylcarnitine, consistently emerged as risk factors across all RCC subtypes. Carnitine facilitates fatty acid transport into mitochondria for β-oxidation, a critical process for energy production in hypoxic tumors [45]. In ccRCC, this process is further amplified by VHL loss, which stabilizes HIF-α and upregulates lipid metabolism genes, leading to lipid droplet accumulation and a dependency on FAO for survival [46]. Similarly, sphingosine 1-phosphate (S1P), elevated in both overall RCC (OR = 1.213) and ccRCC (OR = 1.443), promotes angiogenesis and immune evasion through HIF-α-mediated S1P receptor signaling, further reinforcing its role in ccRCC's hypoxic niche [47]. In pRCC, metabolic divergence is marked by glucuronate (OR = 2.010), a key player in xenobiotic detoxification via UDP-glucuronosyltransferase (UGT) enzymes [48]. Elevated glucuronate suggests compensatory detoxification of reactive oxygen species (ROS) generated by MET proto-oncogene-driven proliferation [49]. The marked increase in the alpha-ketoglutarate-to-alanine ratio (OR = 2.124) highlights a shift toward reductive glutamine metabolism, where alpha-ketoglutarate replenishes TCA cycle intermediates to sustain nucleotide synthesis. At the same time,

alanine accumulation may indicate heightened glycolysis to meet energy demands in MET-altered tumors. ChRCC displays a unique reliance on γ-glutamylthreonine (OR = 2.903), a product of the gamma-glutamyl cycle involved in glutathione synthesis [40]. This implicates chronic oxidative stress and compensatory glutathione production to mitigate ROS damage, consistent with chRCC's oncocytic morphology, characterized by mitochondrial hyperplasia [40]. Additionally, the AMP-to-glutamine ratio (OR = 2.876) and uridine accumulation (OR = 2.272) reflect a dependency on nucleotide salvage pathways, supporting proliferation in the context of impaired oxidative phosphorylation [50]. In terms of metabolic pathways, our results highlight the importance of the valine, leucine, and isoleucine biosynthesis pathways in ccRCC development, consistent with prior evidence [8, 51, 52]. Moreover, we identified pathways such as pyrimidine metabolism, phenylalanine, tyrosine, tryptophan biosynthesis, riboflavin metabolism, and phenylalanine metabolism as being linked to chRCC. These pathways may influence cancer progression through mechanisms related to DNA replication [53], immune activity [54], and one-carbon metabolism [55].

Validation with clinical samples

To validate our findings, we utilized untargeted metabolomic mass spectrometry to analyze tumors and adjacent normal tissues from patients with ccRCC. This analysis revealed significant alterations in the expression of eight metabolites, which were differentially expressed and causally linked to ccRCC. Four metabolites were identified as upregulated and positively associated with ccRCC development, indicating their potential role as harmful factors in this disease. Acetylcarnitine, a well-established biomarker in various tumors, promotes rapid kidney cancer cell proliferation due to its substantial consumption during tumor growth [56]. S1P, a key lipid involved in numerous biological functions such as cell proliferation, differentiation, angiogenesis, chemotaxis, and migration, mediates resistance to VEGF-directed therapies and inhibits antitumor immunity [57]. Inhibition of S1P has been shown to effectively improve the prognosis of kidney cancer patients [58]. Gamma-glutamylglutamine, an amino acid metabolite, promotes tumor cell proliferation by providing biosynthetic precursors and energy. Additionally, N-acetylcytidine, a modified nucleoside, increase RNA stability and translation efficiency, promoting cancer cell survival, proliferation, and metastasis through alteration in gene expression [59, 60]. Furthermore, we identified three metabolites that were downregulated in tumor tissues and were associated with protective effects against ccRCC development, as indicated by MR analysis. 1-Palmitoyl-2-docosahexaenoyl-GPE (16:0/22:6), expressed at decreased levels, can influence cell membrane structure and signaling functions, thereby impacting kidney cancer cell survival and proliferation [61]. 16a-Hydroxy DHEA 3-sulfate, a steroid hormone metabolite, may disrupt endocrine balance related to sex hormones, potentially inhibiting kidney cancer growth [62, 63]. The reduced expression of gamma-glutamyl-alpha-lysine, involved in protein cross-linking, may lead to extracellular matrix instability, thereby facilitating cancer cell invasion and migration [64]. In addition to these metabolites, trigonelline warrants particular attention. Despite its low expression in kidney cancer tissues, its identification as a genetic risk factor for ccRCC through MR analysis suggests a seemingly paradoxical relationship. This warrants further in-depth research to better understand its specific role in ccRCC.

Therapeutic implications

This study highlights the potential of several metabolites, including carnitine, S1P, and trigonelline, as promising therapeutic targets for kidney cancer treatment. These metabolites are integral to kidney cancer initiation and progression, positioning them as attractive candidates for targeted therapeutic interventions. Strategies aimed at modulating FAO, S1P, or trigonelline metabolism hold considerable therapeutic promise. Specifically, targeting the carnitine receptor or S1P receptor could offer effective treatment options. For instance, S1P receptor antagonists such as VPC23019 have been shown to significantly inhibit kidney cancer cell proliferation and induce apoptosis, suggesting their potential as anti-cancer agents [65, 66]. Similarly, carnitine receptor inhibitors, such as Etomoxir, have demonstrated anti-cancer effects across various tumor types by disrupting FAO pathways, thereby inhibiting kidney

cancer cell growth [67]. These compounds represent promising candidates for the development of more effective, targeted treatments for kidney cancer.

Limitations

Despite the valuable insights provided by this study, several limitations should be acknowledged. First, since the data were derived from European populations, the findings may have limited generalizability to other ethnic or geographic groups due to potential genetic and environmental differences. Second, there was some inconsistency between the metabolites identified in the GWAS database and those detected by mass spectrometry, with discrepancies arising from technical variations. Third, correcting for multiple comparisons in high-dimensional metabolomic data presents a challenge. While we used the Benjamini-Hochberg FDR method to analyze 1,400 metabolites, this approach may have resulted in false negatives due to its conservative nature. To address this, we applied grouped FDR correction by metabolite category and conducted sensitivity analyses (e.g., MR-Egger, weighted median) to support nominally significant results. However, the stringent correction may have masked biologically relevant associations, especially for pleiotropic or subtype-specific metabolites. In addition, the metabolomic validation was limited to ccRCC tissue samples, restricting subtype-level comparisons; future studies should include a broader range of RCC subtypes for validation. Finally, while causal links were identified, the underlying molecular mechanisms remain unclear, and further experimental research is needed to confirm these findings and elucidate the relevant pathways.

Conclusion

This study reveals significant associations between specific metabolites and RCC and its subtypes. Notably, elevated levels of carnitine and trigonelline are closely linked to the development and progression of RCC, while gamma-glutamylthreonine is strongly associated with the pathogenesis of chRCC. Furthermore, metabolites such as S1P, acetylcarnitine, gamma-glutamylglutamine, and N-acetylcytidine show substantial dysregulation in ccRCC tumor tissues. These findings offer novel insights into the metabolic reprogramming that drives RCC and highlight several metabolites as promising biomarkers and therapeutic targets for the early detection and precise treatment of kidney cancer.

Acknowledgements

The authors extend their gratitude to all researchers who contributed by sharing GWAS meta-analysis data pertinent to the exposures and outcomes studied, as well as to those who provided open-source codes, which provided a solid foundation for our extended research. We also extend our deepest thanks to the patients who supported and participated in the study. Their willingness to contribute allowed us to gain invaluable insights into kidney cancer. This project was supported by the National Natural Science Foundation of China (82372883), the National Key R&D Program of China (2022YFB4700904), and Shanghai Priority Research Center Construction Project (20222ZZ01011).

Written informed consent was obtained from all participants in accordance with the Declaration of Helsinki.

Disclosure of conflict of interest

None.

Address correspondence to: Xiaofeng Gao, Linhui Wang and Xiaomin Li, Department of Urology, Changhai Hospital, Naval Medical University, Yangpu District, Shanghai 200433, China. E-mail: gxfdoc@sina.com (XFG); wanglinhui@smmu.edu.cn (LHW); 13166173376@163.com (XML)

References

[1] Hsieh JJ, Purdue MP, Signoretti S, Swanton C, Albiges L, Schmidinger M, Heng DY, Larkin J and Ficarra V. Renal cell carcinoma. Nat Rev Dis Primers 2017; 3: 17009.

[2] Vasudev NS, Wilson M, Stewart GD, Adeyoju A, Cartledge J, Kimuli M, Datta S, Hanbury D, Hrouda D, Oades G, Patel P, Soomro N, Sullivan M, Webster J, Selby PJ and Banks RE. Challenges of early renal cancer detection: symptom patterns and incidental diagnosis rate in a multicentre prospective UK cohort of patients presenting with suspected renal cancer. BMJ Open 2020; 10: e035938.

[3] Cirillo L, Innocenti S and Becherucci F. Global epidemiology of kidney cancer. Nephrol Dial Transplant 2024; 39: 920-928.

[4] Bukavina L, Bensalah K, Bray F, Carlo M, Challacombe B, Karam JA, Kassouf W, Mitchell T, Montironi R, O'Brien T, Panebianco V, Scelo G, Shuch B, van Poppel H, Blosser CD and Psutka SP. Epidemiology of renal cell carcinoma: 2022 update. Eur Urol 2022; 82: 529-542.
[5] Park J, Rho MJ and Park YH. Ambient particulate matter exposure and urologic cancer: a longitudinal nationwide cohort study. Am J Cancer Res 2023; 13: 4755-4766.
[6] Moch H, Amin MB, Berney DM, Compérat EM, Gill AJ, Hartmann A, Menon S, Raspollini MR, Rubin MA, Srigley JR, Hoon Tan P, Tickoo SK, Tsuzuki T, Turajlic S, Cree I and Netto GJ. The 2022 World Health Organization classification of tumours of the urinary system and male genital organs-part A: renal, penile, and testicular tumours. Eur Urol 2022; 82: 458-468.
[7] Fouad YA and Aanei C. Revisiting the hallmarks of cancer. Am J Cancer Res 2017; 7: 1016-1036.
[8] Li C, Tao Y, Chen Y, Wu Y, He Y, Yin S, Xu S and Yu Y. Development of a metabolism-related signature for predicting prognosis, immune infiltration and immunotherapy response in breast cancer. Am J Cancer Res 2022; 12: 5440-5461.
[9] Taeubert MJ, Kuipers TB, Zhou J, Li C, Wang S, Wang T, Tobi EW, Belsky DW, Lumey LH and Heijmans BT; BBMRI-NL Metabolomics consortium. Adults prenatally exposed to the Dutch Famine exhibit a metabolic signature associated with a broad spectrum of common diseases. BMC Med 2024; 22: 309.
[10] Wettersten HI, Aboud OA, Lara PN Jr and Weiss RH. Metabolic reprogramming in clear cell renal cell carcinoma. Nat Rev Nephrol 2017; 13: 410-419.
[11] Liu Y, Ouyang Q and Li Q. A novel brown adipocytes-related gene signature predicts and validates prognosis and immune infiltration of clear cell renal cell carcinoma. Am J Cancer Res 2024; 14: 4286-4305.
[12] Lee G, Han K and Lee SS. Different effect of obesity and metabolic syndrome on prostate cancer by age group. Am J Cancer Res 2022; 12: 3198-3207.
[13] Ding X, Zhang W, Li S and Yang H. The role of cholesterol metabolism in cancer. Am J Cancer Res 2019; 9: 219-227.
[14] Long J, Zhang CJ, Zhu N, Du K, Yin YF, Tan X, Liao DF and Qin L. Lipid metabolism and carcinogenesis, cancer development. Am J Cancer Res 2018; 8: 778-791.
[15] Choi YH, Park YM, Hur KJ, Ha US, Hong SH, Lee JY, Kim SW, Han K, Ko SH and Park YH. Duration of diabetes mellitus and risk of kidney and bladder cancer: a longitudinal nationwide cohort study. Am J Cancer Res 2022; 12: 4050-4061.
[16] Emdin CA, Khera AV and Kathiresan S. Mendelian randomization. JAMA 2017; 318: 1925-1926.
[17] Thanassoulis G and O'Donnell CJ. Mendelian randomization: nature's randomized trial in the post-genome era. JAMA 2009; 301: 2386-2388.
[18] Sun C, Liu C, Liu X, Wu Z, Luo J, Liu R, Wang Y, Lu M, Wang Q, Guo M, Tang Y, Li X and Zheng J. Causal relationship between circulating cytokines and follicular lymphoma: a two-sample Mendelian randomization study. Am J Cancer Res 2024; 14: 1577-1593.
[19] Ke B, Li C and Shang H. Sex hormones in the risk of breast cancer: a two-sample Mendelian randomization study. Am J Cancer Res 2023; 13: 1128-1136.
[20] Feng K, Ren F, Xing Z, Zhao Y, Yang C, Liu J, Shang Q, Wang X and Wang X. Microbiome and its implications in oncogenesis: a Mendelian randomization perspective. Am J Cancer Res 2023; 13: 5785-5804.
[21] Zhang Z, Fang T, Chen L, Ji F and Chen J. Multi-omics Mendelian randomization integrating GWAS, eQTL, and mQTL data identified genes associated with breast cancer. Am J Cancer Res 2024; 14: 1433-1445.
[22] Chen Y, Lu T, Pettersson-Kymmer U, Stewart ID, Butler-Laporte G, Nakanishi T, Cerani A, Liang KYH, Yoshiji S, Willett JDS, Su CY, Raina P, Greenwood CMT, Farjoun Y, Forgetta V, Langenberg C, Zhou S, Ohlsson C and Richards JB. Genomic atlas of the plasma metabolome prioritizes metabolites implicated in human diseases. Nat Genet 2023; 55: 44-53.
[23] Mounier N and Kutalik Z. Bias correction for inverse variance weighting Mendelian randomization. Genet Epidemiol 2023; 47: 314-331.
[24] Lin Z, Deng Y and Pan W. Combining the strengths of inverse-variance weighting and Egger regression in Mendelian randomization using a mixture of regressions model. PLoS Genet 2021; 17: e1009922.
[25] Bowden J, Davey Smith G, Haycock PC and Burgess S. Consistent estimation in Mendelian randomization with some invalid instruments using a weighted median estimator. Genet Epidemiol 2016; 40: 304-314.
[26] Minelli C, Del Greco M F, van der Plaat DA, Bowden J, Sheehan NA and Thompson J. The use of two-sample methods for Mendelian randomization analyses on single large datasets. Int J Epidemiol 2021; 50: 1651-1659.
[27] Storey JD. False discovery rate. International Encyclopedia of Statistical Science 2011; 1: 504-508.

[28] Cohen JF, Chalumeau M, Cohen R, Korevaar DA, Khoshnood B and Bossuyt PM. Cochran's Q test was useful to assess heterogeneity in likelihood ratios in studies of diagnostic accuracy. J Clin Epidemiol 2015; 68: 299-306.
[29] Burgess S and Thompson SG. Interpreting findings from Mendelian randomization using the MR-egger method. Eur J Epidemiol 2017; 32: 377-389.
[30] Ong JS and MacGregor S. Implementing MR-PRESSO and GCTA-GSMR for pleiotropy assessment in Mendelian randomization studies from a practitioner's perspective. Genet Epidemiol 2019; 43: 609-616.
[31] Cheng H, Garrick DJ and Fernando RL. Efficient strategies for leave-one-out cross validation for genomic best linear unbiased prediction. J Anim Sci Biotechnol 2017; 8: 38.
[32] Pang Z, Chong J, Zhou G, de Lima Morais DA, Chang L, Barrette M, Gauthier C, Jacques PÉ, Li S and Xia J. MetaboAnalyst 5.0: narrowing the gap between raw spectra and functional insights. Nucleic Acids Res 2021; 49: W388-W396.
[33] Qu Q, Zeng F, Liu X, Wang Q and Deng F. Fatty acid oxidation and carnitine palmitoyltransferase I: emerging therapeutic targets in cancer. Cell Death Dis 2016; 7: e2226.
[34] Zhao Z, Liu Y, Liu Q, Wu F, Liu X, Qu H, Yuan Y, Ge J, Xu Y and Wang H. The mRNA expression signature and prognostic analysis of multiple fatty acid metabolic enzymes in clear cell renal cell carcinoma. J Cancer 2019; 10: 6599-6607.
[35] Tan SK, Hougen HY, Merchan JR, Gonzalgo ML and Welford SM. Fatty acid metabolism reprogramming in ccRCC: mechanisms and potential targets. Nat Rev Urol 2023; 20: 48-60.
[36] Pirpour Tazehkand A, Salehi R, Velaei K and Samadi N. The potential impact of trigonelline loaded micelles on Nrf2 suppression to overcome oxaliplatin resistance in colon cancer cells. Mol Biol Rep 2020; 47: 5817-5829.
[37] Amjad S, Nisar S, Bhat AA, Shah AR, Frenneaux MP, Fakhro K, Haris M, Reddy R, Patay Z, Baur J and Bagga P. Role of NAD^+ in regulating cellular and metabolic signaling pathways. Mol Metab 2021; 49: 101195.
[38] Maurice NJ. Coordination and regulation of bystander memory T cells. University of Washington; 2021.
[39] Kim JW, Byun MS, Yi D, Lee JH, Jeon SY, Jung G, Lee HN, Sohn BK, Lee JY, Kim YK, Shin SA, Sohn CH and Lee DY; KBASE Research Group. Coffee intake and decreased amyloid pathology in human brain. Transl Psychiatry 2019; 9: 270.
[40] Priolo C, Khabibullin D, Reznik E, Filippakis H, Ogórek B, Kavanagh TR, Nijmeh J, Herbert ZT, Asara JM, Kwiatkowski DJ, Wu CL and Henske EP. Impairment of gamma-glutamyl transferase 1 activity in the metabolic pathogenesis of chromophobe renal cell carcinoma. Proc Natl Acad of Sci U S A 2018; 115: E6274-E6282.
[41] Fujii J, Osaki T, Soma Y and Matsuda Y. Critical roles of the cysteine-glutathione axis in the production of γ-glutamyl peptides in the nervous system. Int J Mol Sci 2023; 24: 8044.
[42] He C, Li Q, Wu W, Liu K, Li X, Zheng H and Lai Y. Ferroptosis-associated genes and compounds in renal cell carcinoma. Front Immunol 2024; 15: 1473203.
[43] Kumari R, Palaniyandi S and Hildebrandt GC. Metabolic reprogramming-a new era how to prevent and treat graft versus host disease after allogeneic hematopoietic stem cell transplantation has begun. Front Pharmacol 2020; 11: 588449.
[44] Bansal A, Sanchez DJ, Nimgaonkar V, Sanchez D, Riscal R, Skuli N and Simon MC. Gamma-glutamyltransferase 1 promotes clear cell renal cell carcinoma initiation and progression. Mol Cancer Res 2019; 17: 1881-1892.
[45] Panov AV, Mayorov VI and Dikalov SI. Role of fatty acids β-oxidation in the metabolic interactions between organs. Int J Mol Sci 2024; 25: 12740.
[46] Xiao H, Qu Y, Li H, Zhang Y, Fei M, Liang C, Yang H and Zhang X. HIF-2α/LINC02609/APOL1-mediated lipid storage promotes endoplasmic reticulum homeostasis and regulates tumor progression in clear-cell renal cell carcinoma. J Exp Clin Cancer Res 2024; 43: 29.
[47] Nagahashi M, Abe M, Sakimura K, Takabe K and Wakai T. The role of sphingosine-1-phosphate in inflammation and cancer progression. Cancer Sci 2018; 109: 3671-3678.
[48] Knights KM, Rowland A and Miners JO. Renal drug metabolism in humans: the potential for drug-endobiotic interactions involving cytochrome P450 (CYP) and UDP-glucuronosyltransferase (UGT). Br J Clin Pharmacol 2013; 76: 587-602.
[49] Sánchez Juménez C, Pacheco Moisés FP, Cano ME, Nava Andrade K, Briones Torres AL and Carbajal Arízaga GG. Folate- and glucuronate-functionalization of layered double hydroxides containing dysprosium and gadolinium and the effect on oxidative stress in rat liver mitochondria. Heliyon 2019; 6: e03111.
[50] Sato Y, Yoshizato T, Shiraishi Y, Maekawa S, Okuno Y, Kamura T, Shimamura T, Sato-Otsubo A, Nagae G, Suzuki H, Nagata Y, Yoshida K, Kon A, Suzuki Y, Chiba K, Tanaka H, Niida A, Fujimoto A, Tsunoda T, Morikawa T, Maeda D, Kume H, Sugano S, Fukayama M, Aburatani H, Sanada M, Miyano S, Homma Y and Ogawa S. Integrated molecular analysis of clear-cell re-

nal cell carcinoma. Nat Genet 2013; 45: 860-867.
[51] Sciacovelli M, Dugourd A, Jimenez LV, Yang M, Nikitopoulou E, Costa ASH, Tronci L, Caraffini V, Rodrigues P, Schmidt C, Ryan DG, Young T, Zecchini VR, Rossi SH, Massie C, Lohoff C, Masid M, Hatzimanikatis V, Kuppe C, Von Kriegsheim A, Kramann R, Gnanapragasam V, Warren AY, Stewart GD, Erez A, Vanharanta S, Saez-Rodriguez J and Frezza C. Dynamic partitioning of branched-chain amino acids-derived nitrogen supports renal cancer progression. Nat Commun 2022; 13: 7830.
[52] Zhu M, Hu Y, Gu Y, Lin X, Jiang X, Gong C and Fang Z. Role of amino acid metabolism in tumor immune microenvironment of colorectal cancer. Am J Cancer Res 2025; 15: 233-247.
[53] Okazaki A, Gameiro PA, Christodoulou D, Laviollette L, Schneider M, Chaves F, Stemmer-Rachamimov A, Yazinski SA, Lee R, Stephanopoulos G, Zou L and Iliopoulos O. Glutaminase and poly (ADP-ribose) polymerase inhibitors suppress pyrimidine synthesis and VHL-deficient renal cancers. J Clin Invest 2017; 127: 1631-1645.
[54] Yao Q, Zhang X, Wang Y, Wang C, Wei C, Chen J and Chen D. Comprehensive analysis of a tryptophan metabolism-related model in the prognostic prediction and immune status for clear cell renal carcinoma. Eur J Med Res 2024; 29: 22.
[55] Gibson TM, Weinstein SJ, Mayne ST, Pfeiffer RM, Selhub J, Taylor PR, Virtamo J, Albanes D and Stolzenberg-Solomon R. A prospective study of one-carbon metabolism biomarkers and risk of renal cell carcinoma. Cancer Causes Control 2010; 21: 1061-1069.
[56] Xiong N, Gao X, Zhao H, Cai F, Zhang FC, Yuan Y, Liu W, He F, Zacharias LG, Lin H, Vu HS, Xing C, Yao DX, Chen F, Luo B, Sun W, DeBerardinis RJ, Xu H and Ge WP. Using arterial-venous analysis to characterize cancer metabolic consumption in patients. Nat Commun 2020; 11: 3169.
[57] Xu G, Yang Z, Sun Y, Dong H and Ma J. Interaction of microRNAs with sphingosine kinases, sphingosine-1 phosphate, and sphingosine-1 phosphate receptors in cancer. Discov Oncol 2021; 12: 33.
[58] Hoefflin R, Harlander S, Abhari BA, Peighambari A, Adlesic M, Seidel P, Zodel K, Haug S, Göcmen B, Li Y, Lahrmann B, Grabe N, Heide D, Boerries M, Köttgen A, Heikenwalder M and Frew IJ. Therapeutic effects of inhibition of sphingosine-1-phosphate signaling in HIF-2α inhibitor-resistant clear cell renal cell carcinoma. Cancers (Basel) 2021; 13: 4801.
[59] Zhang G, Luo W, Lyu J, Yu ZG and Huang G. CNNLSTMac4CPred: a hybrid model for N4-acetylcytidine prediction. Interdiscip Sci 2022; 14: 439-451.
[60] Zhang H, Lu R, Huang J, Li L, Cao Y, Huang C, Chen R, Wang Y, Huang J, Zhao X and Yu J. N4-acetylcytidine modifies primary microRNAs for processing in cancer cells. Cell Mol Life Sci 2024; 81: 73.
[61] Lor C and Hirst LS. Effects of low concentrations of docosahexaenoic acid on the structure and phase behavior of model lipid membranes. Membranes (Basel) 2015; 5: 857-874.
[62] Lee GT, Han CS, Kwon YS, Patel R, Modi PK, Kwon SJ, Faiena I, Patel N, Singer EA, Ahn HJ, Kim WJ and Kim IY. Intracrine androgen biosynthesis in renal cell carcinoma. Br J Cancer 2017; 116: 937-943.
[63] Lappano R, Todd LA, Stanic M, Cai Q, Maggiolini M, Marincola F and Pietrobon V. Multifaceted interplay between hormones, growth factors and hypoxia in the tumor microenvironment. Cancers 2022; 14: 539.
[64] Hu Y, Shao Y, Wu C, Yuan C, Ishimura G, Liu W and Chen S. γ-PGA and MTGase improve the formation of ε-(γ-glutamyl) lysine cross-links within hairtail (Trichiurus haumela) surimi protein. Food Chem 2018; 242: 330-337.
[65] Gupta P, Taiyab A, Hussain A, Alajmi MF, Islam A and Hassan MI. Targeting the sphingosine kinase/sphingosine-1-phosphate signaling axis in drug discovery for cancer therapy. Cancers (Basel) 2021; 13: 1898.
[66] Glueck M, Koch A, Brunkhorst R, Ferreiros Bouzas N, Trautmann S, Schaefer L, Pfeilschifter W, Pfeilschifter J and Vutukuri R. The atypical sphingosine 1-phosphate variant, d16: 1 S1P, mediates CTGF induction via S1P2 activation in renal cell carcinoma. FEBS J 2022; 289: 5670-5681.
[67] Yao CH, Liu GY, Wang R, Moon SH, Gross RW and Patti GJ. Identifying off-target effects of etomoxir reveals that carnitine palmitoyltransferase I is essential for cancer cell proliferation independent of β-oxidation. PLoS Biol 2018; 16: e2003782.